Modeling the effect of toroidal plasma rotation on drift-magnetohydrodynamic modes in tokamaks

I. T. Chapman and S. E. Sharapov
EURATOM/UKAEA Fusion Association, Culham Science Centre, Abingdon, Oxfordshire OX14 3DB, United Kingdom

G. T. A. Huysmans
Association EURATOM-CEA Cadarache, 13108 St. Paul-Lez-Durance, France

A. B. Mikhailovskii
Institute for Nuclear Fusion, RRC Kurchatov Institute, Kurchatov Sqr. 1, Moscow 123182, Russia

(Received 29 March 2006; accepted 18 May 2006; published online 21 June 2006)

A new code, MISHKA-F (Flow), has been developed as an extension of the ideal magnetohydrodynamic (MHD) code MISHKA-1 [Mikhailovskii *et al.*, Plasma Phys. Rep. **23**, 844 (1997)] in order to investigate the linear MHD stability of ideal and resistive eigenmodes with respect to the effects of toroidal rotation in tokamaks in general toroidal geometry with the ion diamagnetic drift effect taken into account. Benchmark test results of the MISHKA-F code show good agreement with analytic theory [A. B. Mikhailovskii and S. E. Sharapov, Plasma Phys. Controlled Fusion **42**, 57 (2000)] for the stability limits of the ideal $n/m=1/1$ internal kink mode. The combined stabilizing effects of the ion diamagnetic drift frequency, ω_{*i}, and the toroidal flow shear are also studied. The ω_{*i} stabilization of the internal kink mode is found to be more effective at finite flow shear. Finite-n ballooning modes are studied in plasmas with the toroidal flow shear effect included. The stabilization of the ballooning modes by toroidal rotation is found to agree well with earlier predictions [Webster *et al.*, Phys. Plasmas **11**, 2135 (2004)]. The effect of high flow shear is analyzed for a sawtoothing discharge typical in the Mega Ampère Spherical Tokamak (MAST) [Sykes *et al.*, Nucl. Fusion **41**, 1423 (2001)]. It is found that the ideal $n=1$ internal kink mode can be stabilized by toroidal rotation at values observed experimentally. [DOI: 10.1063/1.2212401]

I. INTRODUCTION

In order to obtain the maximum fusion yield it is imperative to control the magnetohydrodynamic (MHD) instabilities that can limit plasma performance in a tokamak. A careful assessment of how to control or alleviate such MHD activity is best provided by numerical computations that assess the stability of the plasma. Toroidal rotation velocities in the core as high as half of the ion sound speed can be generated in modern-day spherical tokamaks (STs) by neutral beam injection (NBI). Since this fast plasma rotation can influence the stability of ideal and resistive magnetohydrodynamic instabilities, it is necessary to include the effects of rotation in linear stability analyses. However, our knowledge of MHD stability in rotating plasmas is less comprehensive than for static plasmas. The ideal MHD eigenvalue code, MISHKA-1[1] was developed in order to compute ideal MHD instabilities, and then extended to MISHKA-D[2] (drift MHD) to investigate the finite ion gyroradius stabilizing effect of the ion diamagnetic drift frequency, ω_{*i}. Here we present a further extension to consider the effects of toroidal plasma rotation using a new code, MISHKA-F (flow MHD), which also includes the ω_{*i} effect.

The effects of plasma rotation on different MHD instabilities has been discussed in numerous analytical studies. Resistive wall modes can be stabilized by sufficiently fast toroidal rotation;[3,4] ballooning modes are stabilized by sheared toroidal flows[5–7] and the internal kink mode also exhibits stabilization with toroidal rotation.[8–10] There is also substantial experimental work that suggests stabilization of instabilities due to toroidal rotation. The energy losses due to edge localized modes (ELMs) have been shown to reduce due to momentum input from the NBI directed counter to the plasma current in JT-60U[11,12] and DIII-D.[13] Numerical modeling of the effects of toroidal rotation on MHD stability can help to determine what effect it may have on triggering ELMs.

It has also been shown that sawtooth oscillations are stabilized with increasing toroidal rotation[15] and that the direction of momentum input has a profound impact on the stabilization of the sawteeth in the Joint European Torus (JET),[16] the Tokamak Experiment for Technology Oriented Research (TEXTOR),[17] and the Mega Ampère Spherical Tokamak (MAST).[18] What is more, in spherical tokamaks, toroidal rotation velocities can approach the ion sound speed. In the National Spherical Torus Experiment (NSTX), it has been proposed that sawteeth periods are extended by 2-3 times due to the very fast toroidal rotation of the plasma.[19]

The extension of the MISHKA code to include toroidal flow as discussed here will allow modeling of the effect of toroidal rotation and ion diamagnetic drifts to be analyzed for all the instabilities mentioned above. The effects of toroidal rotation have been included in the MARS[4] and CASTOR-FLOW[14] codes, though the effect of the ion diamagnetic frequency at finite flow is not prescribed in either. The equilibrium employed in MISHKA-F is discussed in Sec. II and

the model and numerical method of application is presented in Sec. III. The MISHKA-F code is benchmarked against analytical results for the effect of toroidal rotation on the $n/m=1/1$ internal kink mode in Sec. IV and on high-n ballooning modes in Sec. V. In order to quantify the experimental relevance of the stabilization effect of the sheared toroidal rotation, a MAST discharge is analyzed in Sec. VI. Finally, conclusions are presented in Sec. VII.

II. EQUILIBRIUM

A. Geometry

We use the coordinate system (s,θ,ϕ) related to the magnetic surfaces with straight magnetic field lines described in Ref. 1. Here $s=(\psi/\psi_{\mathrm{edge}})^{1/2}$ is the radial coordinate marking the magnetic surfaces, $\psi=\psi(s)$ is the function characterizing the poloidal magnetic flux, θ is the poloidal coordinate, and ϕ is the toroidal angle. This coordinate system is specified by representing the equilibrium magnetic field, $\mathbf{B}_0$ in the form

$$\mathbf{B}_0=\nabla\phi\times\nabla\psi+F\nabla\phi, \tag{1}$$

where the function $F=F(s)$ characterizes the toroidal magnetic flux. The contravariant components of $\mathbf{B}_0$, B_0^i $(i=1,2,3)$ satisfy the relations $B_0^1=0$, $B_0^3/B_0^2=q(s)$, where $q(s)$ is the safety factor. According to Eq. (1), the ϕth covariant component of $\mathbf{B}_0$, B_{03}, is given by $B_{03}=F$. On the other hand, it follows from Eq. (1) that $B_0^2=f/J$, where $f=\psi'=\mathrm{d}\psi/\mathrm{d}s$ and J is the Jacobian of the coordinate system. In accordance with the choice of the toroidal angle, ϕ, $g_{33}=R^2$, $g^{33}=1/R^2$, where R is the radial coordinate in the cylindrical coordinate system (R,z,ϕ) and g_{33} and g^{33} are the corresponding components of the metric tensor g_{ik} of the coordinate system (s,θ,ϕ) and the inverse metric tensor g^{ik}. Using the above relations we have $B_0^3=g^{33}$, $B_{03}=F/R^2$, $J=fqR^2/F$, and $B_0^2=F/qR^2$.

According to the equilibrium Ampère law, the equilibrium electric current density, $\mathbf{j}_0$, is expressed in terms of the spatial derivatives of the equilibrium magnetic field, $\mathbf{j}_0=\nabla\times\mathbf{B}_0/\mu_0$, so that

$$j_0^1=0,\quad Jj_0^2=-\frac{1}{\mu_0}\frac{\partial F}{\partial s},$$
$$Jj_0^3=\frac{1}{\mu_0}\left(\frac{\partial}{\partial s}\frac{g_{22}F}{qR^2}-\frac{F}{q}\frac{\partial}{\partial\theta}\frac{g_{12}}{R^2}\right). \tag{2}$$

We consider the plasma rotation to be subsonic, $v_\phi\ll c_s$. Thereby we can neglect the effect of rotation on the equilibrium condition, so taking this condition in the form

$$\mathbf{j}_0\times\mathbf{B}_0=\nabla p_0, \tag{3}$$

where $p_0=p_0(s)$ is the equilibrium plasma pressure.

B. Equilibrium plasma rotation

The equilibrium plasma rotation is governed by the ion equilibrium momentum equation

$$en_0(\mathbf{E}_0+\mathbf{v}_0\times\mathbf{B}_0)-\nabla p_{0i}=0. \tag{4}$$

Here e is the ion charge, $n_0=n_0(s)$ is the equilibrium plasma number density, $\mathbf{E}_0$ is the equilibrium radial electric field, $\mathbf{v}_0$ is the equilibrium plasma velocity, and $p_{0i}=p_{0i}(s)$ is the equilibrium ion pressure. It follows from Eq. (4) that

$$\mathbf{v}_0=\mathbf{v}_{E0}+\mathbf{v}_{*i0}+\mathbf{v}_{\|0}. \tag{5}$$

Here $\mathbf{v}_{E0}$ and $\mathbf{v}_{*i0}$ are the equilibrium cross-field drift velocity and the ion diamagnetic drift velocity, respectively, given by

$$\mathbf{v}_{E0}=\frac{\mathbf{E}_0\times\mathbf{B}_0}{\mathbf{B}_0^2}, \tag{6}$$

$$\mathbf{v}_{*i0}=\frac{1}{en_0\mathbf{B}_0^2}\mathbf{B}_0\times\nabla p_{0i}, \tag{7}$$

while $\mathbf{v}_{\|0}$ is an arbitrary vector directed along the field $\mathbf{B}_0$ so that

$$v_{\|0}=\frac{\mathbf{v}_{\|0}\cdot\mathbf{B}_0}{B_0}. \tag{8}$$

III. MODEL FOR PERTURBATIONS

A. Momentum equations

We take the starting momentum equations in the form

$$\rho_0\frac{\mathrm{d}\mathbf{v}}{\mathrm{d}t}+\nabla\cdot\pi_\Lambda^i=-\nabla\tilde{\mathbf{p}}+\frac{1}{\mu_0}\mathbf{H}. \tag{9}$$

Here $\tilde{\mathbf{p}}$ is the perturbed plasma pressure, the function $\mathbf{H}$ is introduced by (see also Ref. 1)

$$\mathbf{H}=[\nabla\times\mathbf{B}_0]\times\tilde{\mathbf{B}}-\mathbf{B}_0\times[\nabla\times\tilde{\mathbf{B}}], \tag{10}$$

where $\tilde{\mathbf{B}}$ is the perturbed magnetic field, $\rho_0=\rho_0(s)$ is the equilibrium plasma mass density, $\mathrm{d}/\mathrm{d}t=\partial/\partial t+\mathbf{v}_{0i}\cdot\nabla$, $\mathbf{v}_{0i}$ is the equilibrium ion velocity, and π_Λ^i is the ion gyroviscosity tensor.

The time dependence of the perturbations is taken in the form $e^{\lambda t}$. Using the rule of covariant differentiation, $\nabla_l A_i=\partial A_i/\partial x^l-\Gamma_{il}^k A_k$, the sth and θth components of Eq. (9) reduce to

$$\lambda\rho_0\tilde{v}_1=-\rho_0 v_0^3\left(\frac{\partial\tilde{v}_1}{\partial\phi}-2\Gamma_{13}^3\tilde{v}_3\right)-\rho_0 v_0^2\left(\frac{\partial\tilde{v}_1}{\partial\theta}-2\Gamma_{12}^1\tilde{v}_1-2\Gamma_{12}^2\tilde{v}_2\right)-\frac{\partial\tilde{p}}{\partial s}+\frac{H_1}{\mu_0}, \tag{11}$$

$$\lambda\rho_0\tilde{v}_2=-\rho_0 v_0^3\left(\frac{\partial\tilde{v}_2}{\partial\phi}-2\Gamma_{23}^3\tilde{v}_3\right)-\rho_0 v_0^2\left(\frac{\partial\tilde{v}_2}{\partial\theta}-2\Gamma_{22}^1\tilde{v}_1-2\Gamma_{22}^2\tilde{v}_2-2\Gamma_{22}^3\tilde{v}_3\right)-\frac{\partial\tilde{p}}{\partial\theta}+\frac{H_2}{\mu_0}, \tag{12}$$

where Γ_{ij}^k are the Christoffel symbols defined as

$$\Gamma_{ij}^{k}=\frac{1}{2}g^{km}\left(\frac{\partial g_{mi}}{\partial x^{l}}+\frac{\partial g_{ml}}{\partial x^{i}}-\frac{\partial g_{il}}{\partial x^{m}}\right). \tag{13}$$

The functions H_1 and H_2 are expressed in terms of $\tilde{B}^1$. They are given in Ref. 1. The contravariant components of $\mathbf{B}$, B^i $(i=1,2,3)$ are given in Appendix A.

The functions $\tilde{v}_i(i=1,2,3)$ are expressed in terms of the contravariant components $\tilde{v}^i$ by

$$\tilde{v}_1=g_{11}\tilde{v}^1+g_{12}\tilde{v}^2,\quad \tilde{v}_2=g_{21}\tilde{v}^1+g_{22}\tilde{v}^2,\quad \tilde{v}_3=g_{33}\tilde{v}^3. \tag{14}$$

Similarly to Ref. 1, instead of $\tilde{v}^2$ and $\tilde{v}^3$, we use the "optimized" components $\hat{v}^2$ and $\hat{v}^3$ defined by

$$\hat{v}^2=[\tilde{\mathbf{v}}\times\mathbf{B}_0]_1,\quad \hat{v}^3=\frac{\tilde{\mathbf{v}}\cdot\mathbf{B}_0}{\mathbf{B}_0^2}=\frac{\tilde{v}_\parallel}{B_0}. \tag{15}$$

Therefore the parallel projection of Eq. (9) is

$$\lambda\rho_0\mathbf{B}_0^2\hat{v}^3=\beta^3-\mathbf{B}_0\cdot\nabla\tilde{p}-\tilde{B}^1\frac{\partial p_0}{\partial s}-\mathbf{B}_0\cdot(\nabla\cdot\pi^i), \tag{16}$$

where β^3 is given in Appendix A.

Then the functions $\tilde{v}_1$, $\tilde{v}_2$, and $\tilde{v}_3$ entering Eqs. (11), (12), and (16) are expressed in terms of $\tilde{v}^1$, $\hat{v}^2$, and $\hat{v}^3$ by

$$\begin{aligned}\tilde{v}_1&=\left(g_{11}-\frac{g_{12}^2F^2}{q^2R^2\mathbf{B}_0^2}\right)\tilde{v}^1+\frac{g_{12}F^2}{fqR^2\mathbf{B}_0^2}\hat{v}^2+\frac{g_{12}F}{qR^2}\hat{v}^3,\\ \tilde{v}_2&=\frac{g_{12}F^2}{R^2\mathbf{B}_0^2}\tilde{v}^1+\frac{g_{22}F^2}{fqR^2\mathbf{B}_0^2}\hat{v}^2+\frac{g_{22}F}{qR^2}\hat{v}^3,\\ \tilde{v}_3&=-\frac{F^2}{qR^2\mathbf{B}_0^2}\left(g_{12}\tilde{v}^1+\frac{g_{22}}{fq}\hat{v}^2\right)+F\hat{v}^3.\end{aligned} \tag{17}$$

The perturbed magnetic fields $\tilde{B}^i$ are expressed in terms of the perturbed vector potential $\mathbf{A}$ by $\mathbf{B}=\nabla\times\mathbf{A}$. The vector potential $\mathbf{A}$ is characterized by the covariant components A_1, A_2 and A_3. Following Ref. 1, instead of the components A_2 and A_3, we use the "optimized components" $\hat{A}_2$ and $\hat{A}_3$ defined by

$$\hat{A}_2=\frac{[\mathbf{A}\times\mathbf{B}_0]^1}{\mathbf{B}_0^2},\quad \hat{A}_3=\tilde{\mathbf{A}}\cdot\mathbf{B}_0=\frac{A_\parallel}{B_0}. \tag{18}$$

In MISHKA-D,[2] the assumption that $\hat{A}_3=0$ is made. However, in the presence of toroidal plasma rotation this is not usually the case so MISHKA-F allows for the finiteness of $\hat{A}_3$. The expressions for the functions $\tilde{B}^i$ $(i=1,2,3)$ in terms of the variables A_1, $\hat{A}_2$, and $\hat{A}_3$ are given in Appendix A.

In calculating the perturbed plasma pressure $\tilde{p}$ we neglect the perturbations of the ion and electron temperatures for simplicity, taking

$$\tilde{p}=(T_{0i}+T_{0e})\tilde{n}. \tag{19}$$

Here T_{0e} is the equilibrium electron temperature. As a result, Eqs. (11), (12), and (16) contain seven variables, viz., $\tilde{v}^1,\hat{v}^2,\hat{v}^3,A_1,\hat{A}_2,\hat{A}_3$, and $\tilde{p}$. Therefore we supplement the momentum equations by four other equations. This is the goal of the next step.

B. Perturbed Ohm's law

We take the perpendicular Ohm's law in the form

$$\tilde{\mathbf{E}}_\perp+[\mathbf{v}_0\times\tilde{\mathbf{B}}]_\perp+[\tilde{\mathbf{v}}\times\mathbf{B}_0]_\perp-\frac{T_{0i}\nabla_\perp\tilde{n}}{en_0}+\frac{\tilde{n}}{en_0^2}\nabla p_{0i}=0, \tag{20}$$

where e is the ion charge. Similarly, the parallel Ohm's law is represented in the form

$$\tilde{E}_\parallel+[\mathbf{v}_0\times\tilde{\mathbf{B}}]_\parallel+\frac{T_{0e}\nabla_\parallel\tilde{n}}{en_0}=0. \tag{21}$$

Here $\perp$ and $\parallel$ represent the directions perpendicular and parallel to the equilibrium magnetic field, respectively. The perturbed electric field is related to the vector potential $\mathbf{A}$ by $\tilde{\mathbf{E}}=-\partial\mathbf{A}/\partial t$. Therefore, for $\partial/\partial t\to\lambda$, we have

$$\tilde{\mathbf{E}}=-\lambda\mathbf{A}. \tag{22}$$

It follows from Eqs. (20)–(22) that

$$\begin{aligned}\lambda A_1=\hat{v}^2&-\left(v_0^3\frac{\partial}{\partial\phi}+v_0^2\frac{\partial}{\partial\theta}\right)A_1-v_0^3\frac{\partial}{\partial s}(f\hat{A}_2)+v_0^2\frac{\partial}{\partial s}(fq\hat{A}_2)\\&+v_0^3\frac{\partial}{\partial s}(F\hat{A}_3)+v_0^2\frac{\partial}{\partial s}\left(\frac{g_{22}F}{qR^2}\hat{A}_3\right)-\frac{T_{0i}}{e}\frac{\partial}{\partial s}\left(\frac{\tilde{n}}{n_0}\right),\end{aligned} \tag{23}$$

$$\begin{aligned}\lambda\hat{A}_2=&-\tilde{v}^1-\frac{v_0^3F}{J\mathbf{B}_0^2}\left[-f\left(\frac{\partial}{\partial\theta}+q\frac{\partial}{\partial\phi}\right)\hat{A}_2\right.\\&\left.+F\left(\frac{\partial}{\partial\theta}-\frac{g_{22}}{qR^2}\frac{\partial}{\partial\phi}\right)\hat{A}_3\right]-\frac{v_0^2Fg_{12}}{J\mathbf{B}_0^2}\\&\times\left[\frac{\partial}{\partial s}(fq\hat{A}_2)-\frac{\partial A_1}{\partial\theta}+\frac{\partial}{\partial s}\left(\frac{g_{22}F\hat{A}_3}{qR^2}\right)\right]\\&-\frac{T_{0i}}{en_0J\mathbf{B}_0^2}\left(\frac{\partial}{\partial\theta}-\frac{g_{22}}{qR^2}\frac{\partial}{\partial\phi}\right)\tilde{n},\end{aligned} \tag{24}$$

$$\begin{aligned}\lambda\mathbf{B}_0^2\hat{A}_3=&\frac{(v_0^3-qv_0^2)F^2}{qR^2}\left[-\frac{f}{F}\left(\frac{\partial}{\partial\theta}+q\frac{\partial}{\partial\phi}\right)\hat{A}_2\right.\\&\left.+\left(\frac{\partial}{\partial\theta}-\frac{g_{22}}{qR^2}\frac{\partial}{\partial\phi}\right)\hat{A}_3\right]+\frac{1}{en_0}(p_{0e}'\tilde{B}^1+T_{0e}\tilde{B}_0\cdot\nabla\tilde{n}).\end{aligned} \tag{25}$$

C. Pressure equation

We start from the pressure equation of the form

$$\lambda\tilde{p}=-\nabla\cdot(p_0\tilde{\mathbf{v}}+\tilde{p}\mathbf{v}_0)-\Gamma\nabla\cdot(p_0\tilde{\mathbf{v}}+\tilde{p}\mathbf{v}_0). \tag{26}$$

Hence we find

$$\lambda\tilde{p} = -\left(v_0^3\frac{\partial}{\partial\phi} + v_0^2\frac{\partial}{\partial\theta}\right)\tilde{p} - \Gamma\tilde{v}^1 p_0' - \Gamma\frac{p_0}{J}\left[F\left(\frac{\partial}{\partial\theta} - \frac{g_{22}}{qR^2}\frac{\partial}{\partial\phi}\right)\frac{\hat{v}^2}{\mathbf{B}_0^2} + \frac{\partial}{\partial s}\left(J\tilde{v}^1\right) - \frac{fF}{q}\left(\frac{\partial}{\partial\theta} + q\frac{\partial}{\partial\phi}\right)\frac{g_{12}\tilde{v}^1}{R^2\mathbf{B}_0^2}\right]. \quad (27)$$

D. Description of numerical method

In the numerical scheme we introduce the "canonical" variables

$$X_1 = fq\tilde{v}^1, \quad X_2 = i\hat{v}^2, \quad X_3 = iA_1, \quad X_4 = fq\hat{A}_2, \quad X_5 = F\hat{A}_3, \quad X_6 = i\hat{v}^3 \quad X_7 = f\tilde{p}. \quad (28)$$

The functions X_i are Fourier expanded in the toroidal and poloidal angles, while the radial structure is described by cubic and quadratic Hermite finite elements, $H(s)$:

$$X = e^{\lambda t}e^{in\phi}\sum_{m=-\infty}^{\infty} e^{im\theta}\sum_{\nu=1}^{N}(X_m)_\nu H_\nu(s), \quad (29)$$

where X is any of the functions in Eq. (28). In order to follow the approach described in Ref. 20, the weak forms are constructed by multiplying Eqs. (11), (12), (16), (23)–(25), and (27) by $\tilde{v}^{1*}$, $\hat{v}^{2*}/fq$, $\mathbf{B}_0^2\hat{v}^{3*}$, A_1^*, $fq\mathbf{B}_0^2\hat{A}_2^*$, $\hat{A}_3^*$, and $f\tilde{p}$, respectively, and integrating over the volume $J\mathrm{d}s\mathrm{d}\theta\mathrm{d}\phi$. The weak forms are given in Appendix B. The set of equations solved by MISHKA-F is given by Eqs. (B1), (B2), (B26), (B36), (B46), (B55), and (B64).

IV. TOROIDAL FLOW STABILIZATION OF THE INTERNAL KINK MODE

A. Flow effects

As a benchmark case for the MISHKA-F code, the stabilization of the $n=1$ internal kink mode with respect to toroidal velocity is analyzed. Analytically, the growth rate of the internal kink mode as a function of the toroidal velocity can be found by using Eq. (3.17) of Ref. 21:

$$\Omega = \frac{\omega_{*i}}{2} \pm \frac{1}{2}(1-\kappa^2)^{1/2}\left[\omega_{*i}^2 - 4(1-\kappa^2)\Lambda^2\omega_A^2\right]^{1/2}, \quad (30)$$

where Ω is the shifted mode frequency, $\Omega=\omega-v_E(r_0)k_y$, ω is the mode frequency, ω_{*i} is the ion diamagnetic frequency, $\omega_A=sv_A/qR$ is the Alfvén frequency, $\Lambda=qR\hat{\gamma}/v_A s$, and

$$\hat{\gamma}^2 = -\frac{1}{(1-\kappa^2)^2}\left[\Omega(\Omega-\omega_{*i}) + \frac{\kappa^2\omega_{*i}^2}{4}\right]. \quad (31)$$

The dimensionless parameter κ is the normalized velocity shear,

$$\kappa = \frac{qR}{sv_A}\frac{\mathrm{d}}{\mathrm{d}r}\left(\frac{rv_T}{Rq}\right) = \frac{R\Omega_\phi}{v_A}\left(\frac{1}{s}-1\right) + \frac{Rq}{v_A}\frac{\mathrm{d}\Omega_\phi}{\mathrm{d}q}, \quad (32)$$

where $v_A=B/\sqrt{n_0M_i}$, v_T is the toroidal rotation prescribed as a profile input to MISHKA-F, $k_y=m/r$, B is the equilibrium magnetic field, n_0 is the plasma density, M_i is the mass of the ions, m is the poloidal mode number, Ω_ϕ is the angular velocity, and s is the magnetic shear, $s=r/qdq/dr$ evaluated at the $q=1$ surface. Here we ignore the diamagnetic effects, so $\omega_{*i}=0$. As such, the flow-shear stabilization of the $n=1$ internal kink mode is described by

$$\Omega = \pm i(1-\kappa^2). \quad (33)$$

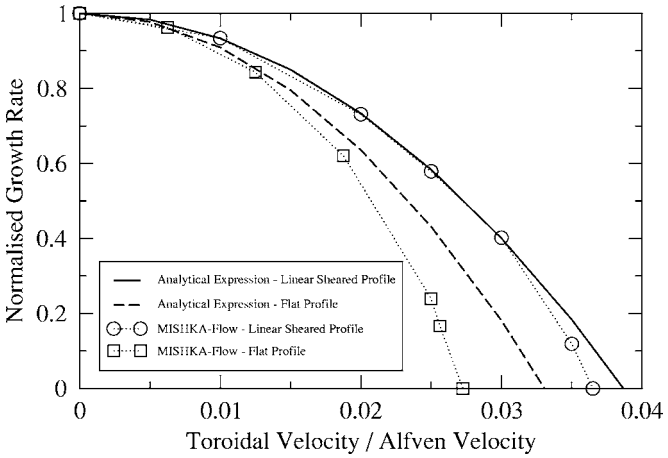

FIG. 1. The growth rate of the $n=1$ internal kink mode as a function of toroidal velocity with flat and linearly sheared rotation profiles. Also shown for comparison is the predicted stabilization from Ref. 21.

MISHKA-F was tested by varying the toroidal velocity with both a constant rotation profile and a linearly sheared rotation profile.

The equilibrium employed [generated by the equilibrium code HELENA[22]] has a pressure profile, $p'=p'(0)\times(1-\psi)$ and a current profile, $\langle j\rangle=j(0)(1-\psi)$, where ψ is normalized poloidal flux. The plasma has a circular boundary, an inverse aspect ratio of 0.1, safety factor on-axis of $q(0)=0.8$, and poloidal beta of $\beta_p=0.3$. The equilibrium is static and unstable to the ideal $n=1$ internal kink mode. Figure 1 shows the growth rate, $\gamma=\mathrm{Re}(\lambda)$, of the internal kink mode normalized to unity as a function of the toroidal velocity normalized to the Alfvén speed, which is in good accordance with Eq. (33). The growth rate of the mode decreases as the toroidal velocity increases, whether the flow is sheared or constant. As the flow reaches $\kappa=1$, the mode is stabilized. The value of flow required to stabilize the internal kink mode is within 15% of the analytical predictions based on considering the inertial layer only. The $n=1$ internal kink mode is stabilized by flows of the order $v_\phi/c_s<0.15$, for which it has been shown[14] that a static equilibrium is an appropriate approximation.

B. Ion diamagnetic effects at finite flow

Now we return to Eq. (30) in order to consider the stabilizing effect of the ion diamagnetic frequency at finite flow shear. It follows that for weak cross-field velocity shear, $\kappa<1$, the ω_{*i} effect is stabilizing, and the $n=1$ internal kink eigenmodes become stable according to analytic theory at

TABLE I. The marginal stability of the $n=1$ internal kink mode with respect to the ion diamagnetic frequency at different toroidal flows. α_1 represents the analytical predictions whereas α_2 is produced by MISHKA-F.

v_0/v_A	α_1	α_2
0.01	0.953	0.826
0.02	0.792	0.677
0.03	0.617	0.527

$$\alpha_1 = \sqrt{1-\kappa^2}, \tag{34}$$

where $\alpha_1 = \omega_{*i}/2\Lambda\omega_A$ and Λ is defined in Ref. 21. In order to compare the value of α_1 at marginal stability given analytically by Eq. (34) with MISHKA-F, we define the value for marginal stability from computational analysis as:

$$\alpha_2 = \frac{\tau^{\text{crit}}(\kappa)}{\tau_0^{\text{crit}}}, \tag{35}$$

where $\tau^{\text{crit}}(\kappa)$ is the critical value of the parameter τ (which represents the ω_{*i} effects, as defined below) corresponding to the stability boundary for finite κ and $\tau_0^{\text{crit}} = \tau^{\text{crit}}(0)$. The dimensionless parameter τ is defined as

$$\tau = \frac{1}{\omega_{Bi}\tau_A} = \frac{1}{e_i R_M}\sqrt{\frac{M_i}{\mu_0 n_{0i}}}, \tag{36}$$

where e_i is the ion charge, n_{0i} is the ion density on axis, $\tau_A = R_0/v_A(0)$, and $v_A(0) = B_0(0)/\sqrt{\mu_0\rho_0(0)}$ is the Alfvén velocity at the magnetic axis. For the equilibrium described above, the stability boundary predicted analytically (represented by α_1) and that found in MISHKA-F (α_2) at different values of the flow shear is given in Table I. This shows a qualitative agreement between theory and numerical predictions, although an exact agreement is not found here since the theory is based upon local approximation of the magnetic shear at the $q=1$ surface whereas the internal kink mode is essentially nonlocal. The $n=1$ internal kink mode can be stabilized by the ω_{*i} effect at any flow shear. When the rotation is directed in the co-current direction, the two effects are aligned and so stabilization is increased. Conversely, when the rotation is directed counter-current, the toroidal rotation is opposed to the ion diamagnetism, and so ω_{*i} needs to be larger to cause stabilization of the mode. This effect is shown in Fig. 2.

Finally, the trajectory of the growth rate, $\gamma = \text{Re}(\lambda)$, and the frequency, $\omega = \text{Im}(\lambda)$, of the $n=1$ internal kink mode as a function of τ is shown in Fig. 3. The behavior of the modes is in good accordance with Eq. (30). At $\tau=0$ (i.e., when there is no ion diamagnetic frequency), two modes exist: one unstable and the other stable and damped, both with the same mode structure. When there is no flow shear, as τ increases the frequency of both modes increases linearly with ω_{*i}, while the growth and damping rates decrease. Eventually, the two modes coalesce, and further increases in τ lead to two stable modes, with increasing and decreasing frequency, respectively. When the flow shear is included this behavior changes, dependent upon the direction of the toroidal rotation. If the rotation is directed in the same direction as ω_{*i} (i.e., co-current rotation), then the growth and damping rates

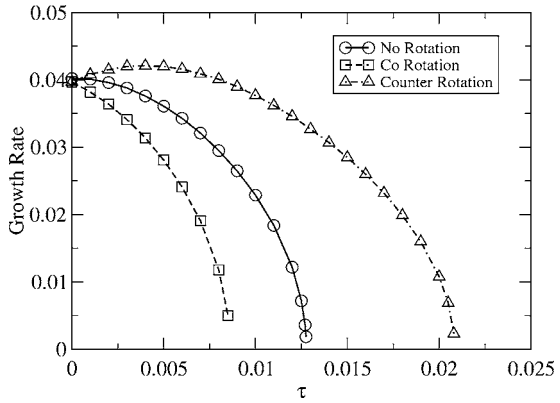

FIG. 2. The growth rate of the $n=1$ internal kink mode as a function of ω_{*i} [here represented by parameter τ given by Eq. (36)] at different orientations of low flow shear.

of the two modes reach zero at a lower value of the ion diamagnetism. This also occurs at a lower frequency than for the static case. Conversely, if the rotation is directed in the opposite direction to ω_{*i}, then the growth and damping rates of the two modes initially increase with τ, before ultimately decreasing as before. Now it requires a higher τ to cause both modes to be stabilized. After stabilization, increasing τ causes a bifurcation of the modes into two stable modes with increasing and decreasing frequency, respectively, as exhibited with no flow shear.

V. TOROIDAL FLOW STABILIZATION OF BALLOONING MODES

The influence of toroidal flow shear on finite-n ballooning modes is analyzed and compared to analytic theory as another benchmark test of MISHKA-F. Ideal MHD predicts that ballooning modes—instabilities which minimize the bending of magnetic field lines—are unstable in regions of high pressure gradients. The highest pressure gradients in a tokamak plasma are found in transport barriers established in high confinement mode (H mode).[23] There are also strong flow shears at such transport barriers, which emphasizes the importance of understanding how flow shear affects the stability of ballooning modes. Ballooning mode stability at an

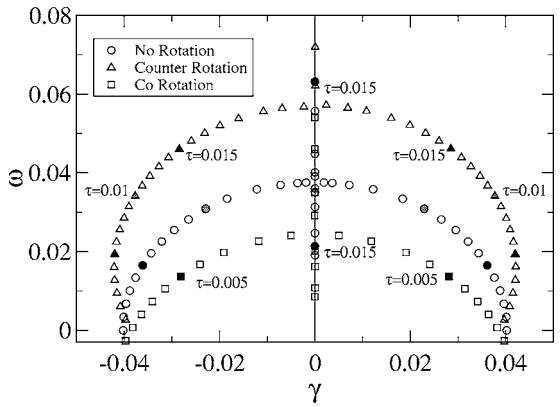

FIG. 3. The trajectory of the growth rate, γ, and the frequency, ω, of the $n=1$ internal kink mode as a function of ω_{*i} [here represented by parameter τ given by Eq. (36)].

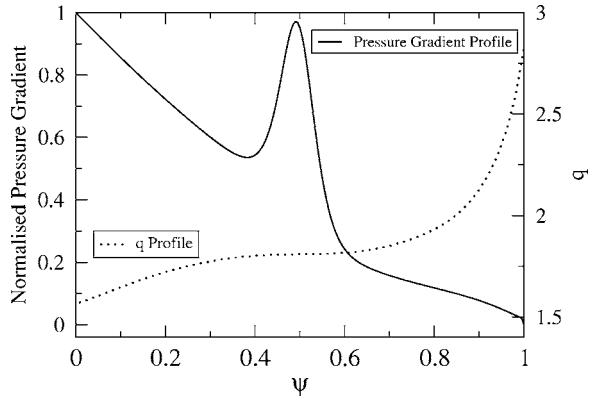

FIG. 4. The steep localized pressure gradient representing the internal transport barrier and the q profile of this equilibrium. The q profile is altered slightly in the vicinity of the ITB as the magnetic shear is changed.

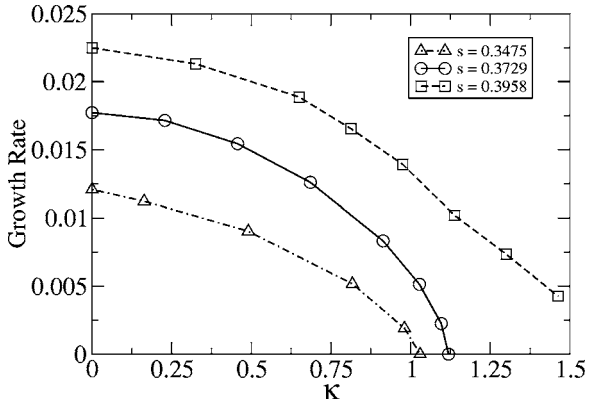

FIG. 5. The growth rate of the ballooning modes at an ITB as a function of dimensionless parameter κ quantifying the sheared toroidal rotation, $\kappa = qR/Sv_A \times \mathrm{d}/\mathrm{d}r(rv_T/Rq)$.

internal transport barrier (ITB) with respect to the sheared toroidal flow was predicted in Ref. 24, where it is suggested that the flow shear will become important when

$$\Delta v \geqslant v_A s \frac{\Delta r}{r}, \tag{37}$$

where Δr is the width of the ITB and Δv is the change in the flow speed over the ITB. This means that the effect of flow becomes more significant at low magnetic shear.

In order to verify the flow effect on ballooning modes, a test case was prescribed by a circular equilibrium characterized by an aspect ratio $R_0/a=3$, safety factor at the boundary, $q_a=3$, and a poloidal beta $\beta_p=0.4$. The equilibrium has a steep localized pressure gradient as shown in Fig. 4 and is unstable to ballooning modes but stable to Mercier modes. In order to reduce the magnetic shear, the q profile is flattened by tailoring the current profile supplied to HELENA.[25]

Figure 5 shows the growth rate of the ballooning modes as a function of the parameter κ representing the sheared toroidal flow. In good accordance with Eq. (33), the growth rate reaches zero when $\kappa \approx 1$. Here the magnetic shear and the flow shear are evaluated at the radial position at which the ballooning mode is most unstable. As the sheared toroidal rotation is increased, the ballooning mode eigenfunction narrows in radial extent, as shown in Figs. 6 and 7. This is consistent with the predictions made in Ref. 24. This narrowing of the mode structure continues to the point when κ is sufficiently high to stabilize the mode, at which point the eigenfunction disappears. In this case, the low magnetic shear means that $\kappa \sim 1$ can be reached with low toroidal flows, $v_\phi/c_s < 0.1$, which satisfies the criterion for the use of a static equilibrium.

VI. STABILITY OF IDEAL MHD MODES IN MAST PLASMAS

As the power of the NBI applied to tokamak plasmas is increased, the quiescent time between sawtooth crashes lengthens.[15] The beam injection leads to momentum input

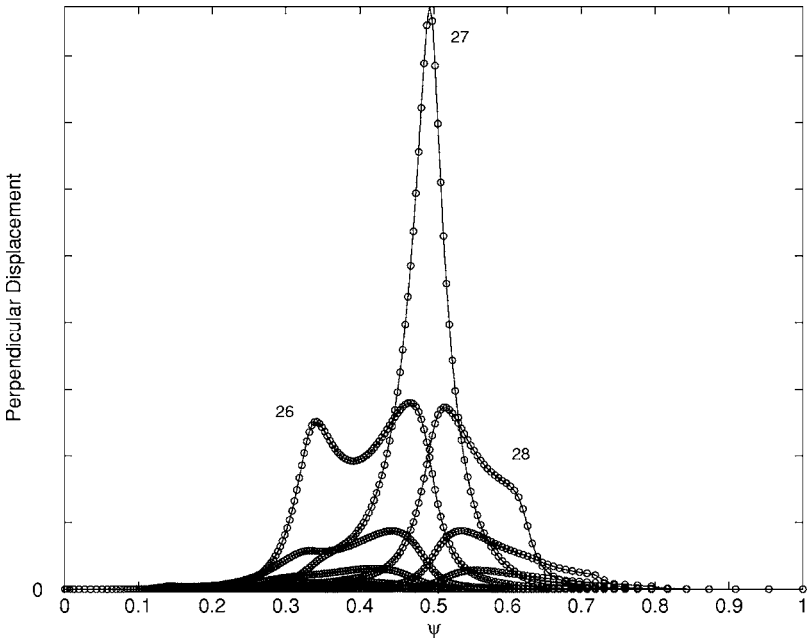

FIG. 6. Radial mode structure (poloidal harmonics) of $n=20$ MHD unstable ballooning mode localized at the internal transport barrier with no toroidal flow.

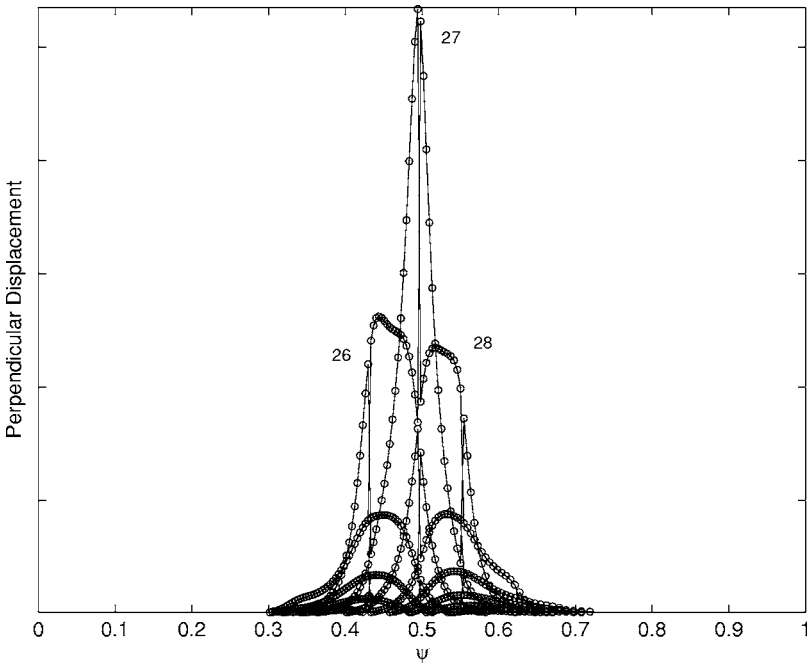

FIG. 7. Radial mode structure (poloidal harmonics) of $n=20$ MHD unstable ballooning mode localized at the internal transport barrier with high toroidal flow, $\kappa \sim 0.8$. The eigenmode has narrowed by approximately 40%.

which can make the plasma spin at speeds approaching the ion sound speed in spherical tokamaks. Recent theoretical work has established that toroidal plasma rotation up to sonic flow speeds has a strong stabilizing effect on internal kink modes.[8,9] MISHKA-F is applied to a typical sawtoothing discharge in MAST with high co-NBI. The plasma is in double null configuration with inverse aspect ratio $\epsilon=0.675$, poloidal beta, $\beta_p=0.42$, magnetic field, $B_t=0.48$ T, and total plasma current, $I_p=763$ kA. The equilibrium has a monotonic q profile with $q_0=0.837$. The growth rate of the ideal $n/m=1/1$ internal kink mode with respect to the toroidal rotation speed is show in Fig. 8. The internal kink mode is completely stabilized by the effect of the toroidal rotation, with the strongest stabilization exhibited with a constant rotation profile. Experimentally, the core rotation speed is approximately 125 km/s, so it can be seen that the stabilization of the internal kink mode occurs at rotation speed of the order of magnitude of those achievable in MAST plasmas with high injected beam power. In this discharge the ion sound speed is approximately 650 km/s so the internal kink mode is stabilized by flows of the order $v_\phi/c_s \sim 0.15$. The rotation profile measured experimentally by the charge exchange diagnostic has been approximated by a polynomial of the form $v(s)=v_0[0.6406+1.6425s-0.564s^2+9.5009s^3+6.6498s^4]$, where v_0 is the rotation velocity in the core. The stronger stabilization provided by a constant rotation profile suggests that the important parameter in the flow-stabilizing mechanism is the amplitude of the flow at the $q=1$ surface. In this equilibrium the $q=1$ surface is at $s=0.4$, and so the constant and linearly sheared rotation profiles cause the kink mode to be stabilized at lower flow speeds than the MAST rotation profile since they are at their maximum in the core, and so the value at the $q=1$ surface is high. The experimental rotation profile is approximately 2/3 of its maximum value in the core and reaches a peak at $r>r(q=1)$. It is evident that the rotation profile and, specifically, the flow shear at $q=1$ is an important parameter when considering the stabilization of the internal kink mode with respect to toroidal rotation. The MISHKA-F results indicate that a strong effect of toroidal and ω_{*i} rotation modifies the linear growth rate of sawteeth, which may be the primary reason for the increased quiescent time between sawteeth and longer sawtooth-free periods observed in strongly co-NBI heated plasmas. Previous theoretical work[10] has shown kinetic stabilization of the ideal $n=1$ internal kink mode by the injected fast ions. Kinetic modeling, which will be addressed in the future, will aim to assess the contribution made by the kinetic effects to the stabilization of the $n=1$ internal kink mode.

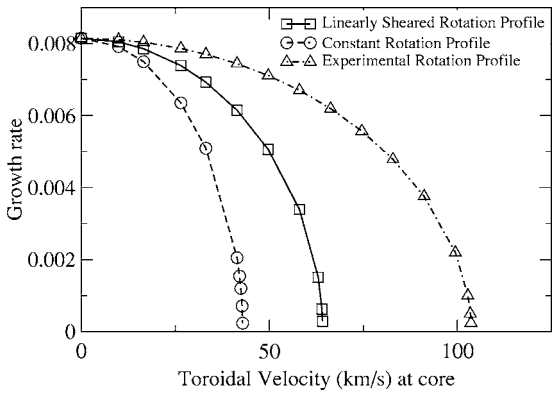

FIG. 8. The growth rate of the ideal $n=1$ internal kink mode as a function of the core toroidal rotation speed for a MAST-like equilibrium.

VII. SUMMARY

The MISHKA-type MHD code[1] has been developed to include the effects of toroidal rotation, which is important for tokamaks such as the ST and the edge plasma in conven-

tional aspect ratio machines, where plasma rotation speeds approaching the ion sound speed are achievable. The equations that extend the ideal one-fluid MHD model to include the effects of toroidal flows have been presented here. The new code, MISHKA-F, allows us to perform computation of both stable and unstable eigenmodes up to a very large toroidal mode number ($n<50-100$) in full toroidal geometry. The stabilization of the $n=1$ internal kink mode and high-n ballooning modes by sheared toroidal flow in a large aspect ratio circular plasma shows good agreement with analytic theory. The internal kink modes are stabilized when the dimensionless parameter, $\kappa=qR/Sv_A\times \mathrm{d}/\mathrm{d}r(rv_T/Rq)$ is equal to one, as are the high-n ballooning modes. The stabilizing influence of the ion diamagnetic frequency, ω_{*i}, at finite toroidal flow shear has also been analyzed for the $n=1$ internal kink mode, and shows qualitative agreement with theoretical predictions. As the flow shear increases, the diamagnetic effect is more stabilizing and the internal kink mode can be stabilized at significantly lower ω_{*i}.

MISHKA-F has been applied to analyze the stabilizing effect of the flow shear on $n=1$ internal kink modes in a sawtoothing MAST discharge with high co-NBI. It was found that at rotation speeds achievable in MAST the internal kink mode can be completely stabilized.

ACKNOWLEDGMENTS

This work was funded jointly by the United Kingdom Engineering and Physical Sciences Research Council and by the European Communities under the contract of Association between EURATOM and UKAEA. The views and opinions expressed herein do not necessarily reflect those of the European Commission. Thanks to Dr Jack Connor, Dr Samuli Saarelma, and Dr Anthony Webster for useful discussions regarding ballooning mode stabilisation by sheared flows.

APPENDIX A: AUXILIARY FORMULAS FOR SECTION III

The functions $\tilde{B}^i(i=1,2,3)$ are expressed in terms of A_1, $\hat{A}_2$, and $\hat{A}_3$ by

$$\tilde{B}^1=\frac{1}{J}\left[-f\left(\frac{\partial}{\partial\theta}+q\frac{\partial}{\partial\phi}\right)\hat{A}_2+F\left(\frac{\partial}{\partial\theta}-\frac{g_{22}}{qR^2}\frac{\partial}{\partial\phi}\right)\hat{A}_3\right], \quad \text{(A1)}$$

$$\tilde{B}^2=\frac{1}{J}\left[\frac{\partial A_1}{\partial\phi}+\frac{\partial}{\partial s}(f\hat{A}_2)-\frac{\partial}{\partial s}(F\hat{A}_3)\right], \quad \text{(A2)}$$

$$\tilde{B}^3=\frac{1}{J}\left[\frac{\partial}{\partial s}(fq\hat{A}_2)-\frac{\partial A_1}{\partial\theta}+\frac{\partial}{\partial s}\left(\frac{g_{22}F}{qR^2}\hat{A}_3\right)\right]. \quad \text{(A3)}$$

The function β^3 used in Eq. (16) is defined as

$$\begin{aligned}\beta^3=\frac{\rho_0}{\mathbf{B}_0^2}\Bigg[&\frac{Fg_{12}}{qR^2}\left(\left(v_0^2\frac{\partial}{\partial\theta}+v_0^3\frac{\partial}{\partial\phi}+v_0^2 2\Gamma^1_{12}\right)\tilde{v}^1+v_0^2 2\Gamma^1_{22}\tilde{v}^2+v_0^3 2\Gamma^1_{33}\tilde{v}^3\right)+\frac{Fg_{22}}{qR^2}\left(\left(\frac{\partial v_0^2}{\partial s}+v_0^2 2\Gamma^2_{12}\right)\tilde{v}^1\right.\\&+\left(v_0^2\frac{\partial}{\partial\theta}+v_0^3\frac{\partial}{\partial\phi}+\frac{\partial v_0^2}{\partial\theta}+v_0^2 2\Gamma^2_{22}\right)\tilde{v}^2+\left(\frac{\partial v_0^2}{\partial\phi}+v_0^3+v_0^3 2\Gamma^2_{33}\right)\tilde{v}^3\Big)+F\Bigg(\left(\frac{\partial v_0^3}{\partial s}+v_0^3 2\Gamma^3_{31}\right)\tilde{v}^1\\&+\left(\frac{\partial v_0^3}{\partial\theta}+v_0^2 2\Gamma^3_{22}+v_0^3 2\Gamma^3_{32}\right)\tilde{v}^2+\left(v_0^2\frac{\partial}{\partial\theta}+v_0^3\frac{\partial}{\partial\phi}+\frac{\partial v_0^3}{\partial\phi}+v_0^2 2\Gamma^3_{23}\right)\tilde{v}^3\Bigg)\Bigg]. \quad \text{(A4)}\end{aligned}$$

APPENDIX B: WEAK FORMS

1. Momentum equations

We multiply Eqs. (11) and (12) by $\tilde{v}^{1*}$ and $\hat{v}^{2*}/fq$, respectively, and integrate the results over s and θ with the weighting factor J, and substitute Eq. (17) for $\tilde{v}_1$, $\hat{v}_2$, and $\hat{v}_3$ to obtain

$$\lambda\int X_1^*[B(1,1)X_1+B(1,2)X_2+B(1,6)X_6]\mathrm{d}s\mathrm{d}\theta=I_1^A+I_1^P+I_1^F, \quad \text{(B1)}$$

$$\lambda\int X_2^*[B(2,1)X_1+B(2,2)X_2+B(2,6)X_6]\mathrm{d}s\mathrm{d}\theta=I_2^A+I_2^P+I_2^F. \quad \text{(B2)}$$

The matrix $B(k,l)[(k,l)=(1,2)]$ is given in the appendix of Ref. 2. The matrix elements $B(1,6)$ and $B(2,6)$ are given by

$$B(1,6)=i\frac{\rho q}{F^2}R^2(\nabla\psi\cdot\nabla\theta), \quad \text{(B3)}$$

$$B(2,6)=\frac{\rho q}{F^2}R^2|\nabla\psi|^2. \quad \text{(B4)}$$

Here the matrix elements are the coefficients in front of the quadratic combinations of the variables $X_i(i\in[1,7])$. The values I_1^A and I_2^A are defined as

$$\begin{aligned}I_1^A=\int&[A(1,3)X_1^*X_3+A(1',3)X_1^{*\prime}X_3+A(1,4)X_1^*X_4\\&+A(1',4)X_1^{*\prime}X_4+A(1,4')X_1^*X_4'+A(1',4')X_1^{*\prime}X_4'\\&+A(1,5)X_1^*X_5+A(1',5)X_1^{*\prime}X_5+A(1,5')X_1^*X_5']\mathrm{d}s\mathrm{d}\theta,\end{aligned} \quad \text{(B5)}$$

$$I_2^A = \int [A(2,3)X_2^* X_3 + A(2,4)X_2^* X_4 + A(2,4')X_2^* X_4' + A(2,5)X_2^* X_5 + A(2,5')X_2^* X_5']\mathrm{d}s\mathrm{d}\theta. \tag{B6}$$

The matrix elements $A(1,3)$, $A(1',3)$, $A(1,4)$, $A(1',4)$ $A(1,4')$, $A(1',4')$, $A(2,3)$, $A(2,4)$, and $A(2,4')$ can be found in the appendix of Ref. 2 while the other matrix elements entering Eqs. (B1) and (B2) are

$$\begin{aligned} A(1,5) = &-\frac{1}{fF^2}\frac{\mathrm{d}F}{\mathrm{d}s}\left(\frac{\partial|\nabla\psi|^2}{\partial s} + \left(\frac{1}{q}\frac{\mathrm{d}q}{\mathrm{d}s} - \frac{2}{F}\frac{\mathrm{d}F}{\mathrm{d}s}\right)|\nabla\psi|^2\right) \\ &+ \frac{im}{Fq}\frac{\mathrm{d}q}{\mathrm{d}s}(\nabla\psi\cdot\nabla\theta) + \frac{nf}{Fq}(\bar{m}+nq)\frac{1}{R^2} - \frac{mf}{F} \\ &\times(\bar{m}+nq)\left(\frac{(\nabla\psi\cdot\nabla\theta)^2}{|\nabla\psi|^2} + \frac{F^2}{q^2}\frac{1}{R^2|\nabla\psi|^2}\right) \\ &- \frac{in}{F^3}\frac{\mathrm{d}q}{\mathrm{d}s}(\nabla\psi\cdot\nabla\theta)|\nabla\psi|^2 + \frac{nqf}{F^3}(\bar{m}+nq) \\ &\times(\nabla\psi\cdot\nabla\theta)^2, \end{aligned} \tag{B7}$$

$$\begin{aligned} A(1',5) = &\frac{1}{fF}\left(\frac{\partial}{\partial s}|\nabla\psi|^2 + \left(\frac{1}{q}\frac{\mathrm{d}q}{\mathrm{d}s} - \frac{2}{F}\frac{\mathrm{d}F}{\mathrm{d}s}\right)|\nabla\psi|^2\right) \\ &- \frac{im}{F}(\nabla\psi\cdot\nabla\theta) + \frac{inq}{F^3}(\nabla\psi\cdot\nabla\theta)|\nabla\psi|^2, \end{aligned} \tag{B8}$$

$$\begin{aligned} A(1,5') = &\frac{1}{fF}\left(\frac{\partial}{\partial s}|\nabla\psi|^2 + \left(\frac{2}{q}\frac{\mathrm{d}q}{\mathrm{d}s} - \frac{2}{F}\frac{\mathrm{d}F}{\mathrm{d}s}\right)|\nabla\psi|^2\right) \\ &+ \frac{i}{F}(2\bar{m} - m + nq)(\nabla\psi\cdot\nabla\theta), \end{aligned} \tag{B9}$$

$$\begin{aligned} A(2,5) = &\frac{(m-\bar{m})}{f}\frac{\mathrm{d}F}{\mathrm{d}s} + \frac{(m-\bar{m})}{fF}\frac{\mathrm{d}p_0}{\mathrm{d}s}R^2 \\ &- \frac{1}{fF^3}\left((\bar{m}+nq)F\frac{\mathrm{d}F}{\mathrm{d}s} + nq\frac{\mathrm{d}p_0}{\mathrm{d}s}R^2\right)|\nabla\psi|^2 \\ &- \frac{in^2q^2}{F^3}|\nabla\psi|^2(\nabla\psi\cdot\nabla\theta) + \frac{i}{F}(m\bar{m} - \bar{m}^2 + mnq) \\ &\times(\nabla\psi\cdot\nabla\theta), \end{aligned} \tag{B10}$$

$$A(2,5') = \frac{1}{fF}(\bar{m}+nq)|\nabla\psi|^2. \tag{B11}$$

The integrals I_1^p and I_2^p are related to the perturbed plasma pressure and they are defined as

$$I_1^p = \int (X_1^{*\prime} G_{1p}' + X_1^* G_{1p})\mathrm{d}s\mathrm{d}\theta, \tag{B12}$$

$$I_2^p = \int X_2^* G_{2p}\mathrm{d}s\mathrm{d}\theta. \tag{B13}$$

Here

$$G_{1p}' = A(1',7)X_7, \quad G_{1p} = A(1,7)X_7, \quad G_{2p} = A(2,7)X_7 \tag{B14}$$

and the matrix elements in Eq. (B14) are

$$A(1,7) = \frac{1}{fF}\frac{\partial R^2}{\partial s} - \frac{R^2}{fF^2}\frac{\mathrm{d}F}{\mathrm{d}s}, \tag{B15}$$

$$A(1',7) = \frac{R^2}{fF}, \tag{B16}$$

$$A(2,7) = \frac{m}{fF}R^2. \tag{B17}$$

The integrals I_1^F and I_2^F describe the flow effects and are given by

$$I_1^F = \int X_1^*[A^F(1,1)X_1 + A^F(1,2)X_2 + A^F(1,6)X_6]\mathrm{d}s\mathrm{d}\theta, \tag{B18}$$

$$I_2^F = \int X_2^*[A^F(2,1)X_1 + A^F(2,2)X_2 + A^F(2,6)X_6]\mathrm{d}s\mathrm{d}\theta, \tag{B19}$$

where the flow-dependent matrix elements entering Eq. (B1) are given by

$$\begin{aligned} A^F(1,1) = &-i\frac{\rho nfv_0^3}{Fq}\frac{R^2}{|\nabla\psi|^2} - i\frac{\rho nfqv_0^3}{F^3}\frac{R^4(\nabla\psi\cdot\nabla\theta)^2}{|\nabla\psi|^2} \\ &+ i\frac{\rho nfqv_0^3}{F^3}\frac{R^4(\nabla\psi\cdot\nabla\theta)^2}{F^2+|\nabla\psi|^2} \\ &+ \frac{\rho v_0^3}{F}\frac{R^2(\nabla\psi\cdot\nabla\theta)}{F^2+|\nabla\psi|^2}\frac{\partial R^2}{\partial s}, \end{aligned} \tag{B20}$$

$$A^F(1,2) = \frac{\rho nqv_0^3}{F}\frac{R^4(\nabla\psi\cdot\nabla\theta)}{F^2+|\nabla\psi|^2} + i\frac{\rho v_0^3}{fF}\frac{R^2|\nabla\psi|^2}{F^2+|\nabla\psi|^2}\frac{\partial R^2}{\partial s}, \tag{B21}$$

$$A^F(1,6) = \frac{\rho nfqv_0^3}{F^2}R^2(\nabla\psi\cdot\nabla\theta) - i\rho v_0^3\frac{\partial R^2}{\partial s}. \tag{B22}$$

The flow-dependent matrix elements entering Eq. (B2) are

$$A^F(2,1) = -\frac{\rho nqv_0^3}{F}\frac{R^4(\nabla\psi\cdot\nabla\theta)}{F^2+|\nabla\psi|^2} + i\frac{\rho v_0^3}{F}\frac{R^2(\nabla\psi\cdot\nabla\theta)}{F^2+|\nabla\psi|^2}\frac{\partial R^2}{\partial\theta}, \tag{B23}$$

$$A^F(2,2) = -i\frac{\rho nqv_0^3}{fF}\frac{R^4|\nabla\psi|^2}{F^2+|\nabla\psi|^2} - \frac{\rho v_0^3}{fF}\frac{R^2|\nabla\psi|^2}{F^2+|\nabla\psi|^2}\frac{\partial R^2}{\partial\theta}, \tag{B24}$$

$$A^F(2,6) = -i\frac{\rho nqv_0^3}{F^2}R^2|\nabla\psi|^2 + \rho v_0^3\frac{\partial R^2}{\partial\theta}. \tag{B25}$$

We multiply Eq. (16) by $J\mathbf{B}_0^2\hat{v}^{3*}$ and integrate over s and θ to obtain

$$\lambda \int X_6^* B(6,6) X_6 \mathrm{d}s\mathrm{d}\theta = \int X_6^* G_6^p \mathrm{d}s\mathrm{d}\theta + \int X_6^* G_6^A \mathrm{d}s\mathrm{d}\theta + \int X_6^* G_6^F \mathrm{d}s\mathrm{d}\theta, \tag{B26}$$

where

$$G_6^p = A(6,7)X_7 \quad G_6^A = A(6,4)X_4 + A(6,5)X_5 \tag{B27}$$

and the matrix elements are

$$B(6,6) = \rho f q F + \frac{\rho f q}{F}|\nabla\psi|^2, \tag{B28}$$

$$A(6,4) = -(m+nq)\frac{1}{q}\frac{\mathrm{d}p_0}{\mathrm{d}s}, \tag{B29}$$

$$A(6,5) = \frac{\mathrm{d}p_0}{\mathrm{d}s}\left(m - \frac{nq}{F^2}|\nabla\psi|^2\right), \tag{B30}$$

$$A(6,7) = m + nq. \tag{B31}$$

The function G_6^F describes the flow effects and is defined by

$$G_6^F = A^F(6,1)X_1 + A^F(6,2)X_2 + A^F(6,6)X_6. \tag{B32}$$

The matrix elements entering Eq. (B32) are given by

$$\begin{aligned} A^F(6,1) = &-i\rho v_0^3 \frac{\partial R^2}{\partial s} - i\rho f v_0^3 \frac{(\nabla\psi\cdot\nabla\theta)}{F^2+|\nabla\psi|^2}\frac{\partial R^2}{\partial\theta} \\ &- i\frac{\rho f^2 q^2 v_0^3}{F^2}\frac{R^2(\nabla\psi\cdot\nabla\theta)^2}{F^2+|\nabla\psi|^2} \\ &\times\left(\frac{|\nabla\psi|^2}{f^2}\frac{\partial R^2}{\partial s} + \frac{(\nabla\psi\cdot\nabla\theta)}{f}\frac{\partial R^2}{\partial\theta}\right) \\ &+ i\frac{\rho f q^2 v_0^3}{F^2}\frac{|\nabla\psi|^2(\nabla\psi\cdot\nabla\theta)}{F^2+|\nabla\psi|^2} \\ &\times\left(\frac{(\nabla\psi\cdot\nabla\theta)}{f}\frac{\partial R^2}{\partial s} + |\nabla\theta|^2\frac{\partial R^2}{\partial\theta}\right), \end{aligned} \tag{B33}$$

$$\begin{aligned} A^F(6,2) = &-\rho F^2 v_0^3 \frac{1}{F^2+|\nabla\psi|^2}\frac{\partial R^2}{\partial\theta} + \frac{\rho f q^2 v_0^3}{F^2}\frac{R^2(\nabla\psi\cdot\nabla\theta)}{F^2+|\nabla\psi|^2} \\ &\times\left(\frac{|\nabla\psi|^2}{f^2}\frac{\partial R^2}{\partial s} + \frac{(\nabla\psi\cdot\nabla\theta)}{f}\frac{\partial R^2}{\partial\theta}\right) \\ &- \frac{\rho q^2 v_0^3}{F^2}\frac{R^2|\nabla\psi|^4}{F^2+|\nabla\psi|^2} \\ &\times\left(\frac{(\nabla\psi\cdot\nabla\theta)}{f}\frac{\partial R^2}{\partial s} + |\nabla\theta|^2\frac{\partial R^2}{\partial\theta}\right), \end{aligned} \tag{B34}$$

$$\begin{aligned} A^F(6,6) = &-i\frac{\rho n q f v_0^3}{F}(F^2+|\nabla\psi|^2) \\ &- \rho f F v_0^3 \frac{1}{R^2(F^2+|\nabla\psi|^2)}\frac{\partial R^2}{\partial\theta} \\ &+ \frac{\rho f q^2 v_0^3}{F}\frac{|\nabla\psi|^2}{F^2+|\nabla\psi|^2} \\ &\times\left(\frac{(\nabla\psi\cdot\nabla\theta)}{f}\frac{\partial R^2}{\partial s} + |\nabla\theta|^2\frac{\partial R^2}{\partial\theta}\right) \\ &- \frac{\rho f^2 q^2 v_0^3}{F}\frac{(\nabla\psi\cdot\nabla\theta)}{F^2+|\nabla\psi|^2} \\ &\times\left(\frac{|\nabla\psi|^2}{f^2}\frac{\partial R^2}{\partial s} + \frac{(\nabla\psi\cdot\nabla\theta)}{f}\frac{\partial R^2}{\partial\theta}\right). \end{aligned} \tag{B35}$$

2. Perturbed Ohm's law

We multiply Eq. (23) by A_1^* and integrate the result over s,θ to obtain

$$\lambda \int X_3^* B(3,3) X_3 \mathrm{d}s\mathrm{d}\theta = \int A(3,2) X_3^* X_2 \mathrm{d}s\mathrm{d}\theta + \int \tau X_3^* G_3^\tau \mathrm{d}s\mathrm{d}\theta + \int X_3^* G_3^F \mathrm{d}s\mathrm{d}\theta. \tag{B36}$$

The matrix elements $B(3,3)$ and $A(3,2)$ are given in the appendix of Ref. 2. The function G_3^τ is defined as

$$G_3^\tau = A^\tau(3,7')X_7' + A^\tau(3,7)X_7, \tag{B37}$$

where the matrix elements $A^\tau(3,7)$ and $A^\tau(3,7')$ are given by

$$A^\tau(3,7') = -i\frac{T_{0i}}{n_0 f}, \tag{B38}$$

$$A^\tau(3,7) = -iT_{0i}\frac{\partial}{\partial s}\left(\frac{1}{n_0 f}\right). \tag{B39}$$

The function G_3^F describes the flow effect and is defined by

$$G_3^F = A^F(3,3)X_3 + A^F(3,4')X_4' + A^F(3,4)X_4 + A^F(3,5')X_5' + A^F(3,5)X_5. \tag{B40}$$

The matrix elements entering Eq. (B40) are given by

$$A^F(3,3) = -i(nv_0^3 + mv_0^2), \tag{B41}$$

$$A^F(3,4) = -iv_0^3\frac{\mathrm{d}}{\mathrm{d}s}\left(\frac{1}{q}\right), \tag{B42}$$

$$A^F(3,4') = i\left(v_0^2 - \frac{v_0^3}{q}\right), \tag{B43}$$

$$A^F(3,5) = -iv_0^2\frac{\mathrm{d}}{\mathrm{d}s}\left(\frac{g_{22}}{qR^2}\right), \tag{B44}$$

$$A^F(3,5') = i\left(v_0^3 + v_0^2\frac{g_{22}}{qR^2}\right). \tag{B45}$$

Equation (24) is integrated with the weight $A_2^* fqJ\mathbf{B}_0^2$ to obtain

$$\lambda\int X_4^* B(4,4)X_4 \mathrm{d}s\mathrm{d}\theta = \int A(4,1)X_4^* X_1 \mathrm{d}s\mathrm{d}\theta + \tau\int X_4^* G_4^\tau \mathrm{d}s\mathrm{d}\theta + \int X_4^* G_4^F \mathrm{d}s\mathrm{d}\theta. \tag{B46}$$

The matrix elements $B(4,4)$ and $A(4,1)$ are

$$A(4,1) = -B(4,4) = -F\left(1+\frac{g_{22}}{qR^2}\right). \tag{B47}$$

The function G_4^τ is given by

$$G_4^\tau = A^\tau(4,7)X_7, \tag{B48}$$

where $A^\tau(4,7)$ is

$$A^\tau(4,7) = -i\frac{F}{f}\frac{T_{0i}}{n_0}\left(m - nq\frac{|\nabla\psi|^2}{F^2}\right). \tag{B49}$$

The function G_4^F describing the flow effects is given by

$$G_4^F = A^F(4,3)X_3 + A^F(4,4)X_4 + A^F(4,5)X_5 + A^F(4,5')X_5'. \tag{B50}$$

The matrix elements entering Eq. (B50) are given by

$$A^F(4,3) = mv_0^2 F g_{12}, \tag{B51}$$

$$A^F(4,4) = -iv_0^3\frac{F}{q}(m+nq), \tag{B52}$$

$$A^F(4,5) = iv_0^3 F\left(m - \frac{ng_{22}}{qR^2}\right) - v_0^2 F g_{12}\frac{\mathrm{d}}{\mathrm{d}s}\left(\frac{g_{22}}{qR^2}\right), \tag{B53}$$

$$A^F(4,5') = -v_0^2\frac{F g_{12} g_{22}}{qR^2}. \tag{B54}$$

Multiplying Eq. (25) by $A_3^* J = X_5^* J/F$ and integrating the result over s,θ, we obtain

$$\lambda\int X_5^* B(5,5)X_5 \mathrm{d}s\mathrm{d}\theta = \tau\int X_5^* G_5^\tau \mathrm{d}s\mathrm{d}\theta + \int X_5^* G_5^F \mathrm{d}s\mathrm{d}\theta. \tag{B55}$$

The matrix element $B(5,5)$ is

$$B(5,5) = \frac{fq}{F}\left(1+\frac{|\nabla\psi|^2}{F^2}\right). \tag{B56}$$

The function G_5^τ is defined as

$$G_5^\tau = A^\tau(5,4)X_4 + A^\tau(5,5)X_5 + A^\tau(5,7)X_7, \tag{B57}$$

where the matrix elements $A^\tau(5,4)$, $A^\tau(5,5)$, and $A^\tau(5,7)$ are given by

$$A^\tau(5,4) = -i\frac{p_{0e}'}{n_0 F q}(m+nq), \tag{B58}$$

$$A^\tau(5,5) = i\frac{p_{0e}' m}{F n_0} - i\frac{p_{0e}' nq}{F^3 n_0}|\nabla\psi|^2, \tag{B59}$$

$$A^\tau(5,7) = \frac{iT_{0e}}{n_0 F}(m+nq). \tag{B60}$$

The function G_5^F describing the flow effects is defined as

$$G_5^F = A^F(5,4)X_4 + A^F(5,5)X_5, \tag{B61}$$

where the matrix elements $A^F(5,4)$ and $A^F(5,5)$ are given by

$$A^F(5,4) = -i\frac{f(m+nq)}{qF}(v_0^3 - qv_0^2), \tag{B62}$$

$$A^F(5,5) = i\frac{f}{F}\left(m - \frac{ng_{22}}{qR^2}\right)(v_0^3 - qv_0^2). \tag{B63}$$

3. Pressure equation

Multiplying Eq. (26) by JX_7^* and integrating with respect to s,θ, we obtain

$$\lambda\int B(7,7)X_7^* X_7 \mathrm{d}s\mathrm{d}\theta = \int [G_7 X_7^* + G_7' X_7^{*\prime}]\mathrm{d}s\mathrm{d}\theta\int X_7^* G_7^F \mathrm{d}s\mathrm{d}\theta. \tag{B64}$$

The matrix element $B(7,7)$ is

$$B(7,7) = \frac{qR^2}{F}. \tag{B65}$$

The functions G_7 and G_7' are defined as

$$G_7 = A(7,1)X_1 + A(7,2)X_2 + A(7,6)X_6,$$

$$G_7' = A(7',1)X_1, \tag{B66}$$

where the matrix elements entering Eq. (B66) are

$$A(7,1) = (\Gamma-1)\frac{R^2}{F}\frac{\mathrm{d}p_0}{\mathrm{d}s} - i(\bar{m}+nq)\Gamma p_0 f\frac{R^2(\nabla\psi\cdot\nabla\theta)}{F^3 + F|\nabla\psi|^2}, \tag{B67}$$

$$A(7,2) = -\frac{F}{F^2+|\nabla\psi|^2}\Gamma\left(\bar{m} - \frac{nq}{F^2}|\nabla\psi|^2\right)p_0 R^2, \tag{B68}$$

$$A(7,6) = -f\Gamma(\bar{m}+nq)p_0, \tag{B69}$$

$$A(7',1) = p_0\Gamma\frac{R^2}{F}. \tag{B70}$$

The function G_7^F describes the flow effects and is defined by

$$G_F^7 = A^F(7,7)X_7, \tag{B71}$$

where $A^F(7,7)$ is

$$A^F(7,7) = -i(nv_0^3 + mv_0^2)B(7,7). \tag{B72}$$

[1]A. B. Mikhailovskii, G. T. A. Huysmans, W. O. K. Kerner, and S. E. Sharapov, Plasma Phys. Rep. **23**, 844 (1997).
[2]G. T. A. Huysmans, S. E. Sharapov, A. B. Mikhailovskii, and W. O. K. Kerner, Phys. Plasmas **8**, 4292 (2001).
[3]C. G. Gimblett, Nucl. Fusion **26**, 617 (1986).
[4]M. S. Chu, J. M. Greene, T. H. Jensen, R. L. Miller, A. Bondeson, R. W. Johnson, and M. E. Mauel, Phys. Plasmas **2**, 2236 (1995).
[5]R. L. Miller, F. L. Waelbroeck, A. B. Hassam, and R. E. Waltz, Phys. Plasmas **2**, 3676 (1995).
[6]J. W. Connor, R. J. Hastie, and J. B. Taylor, Plasma Phys. Controlled Fusion **46**, B1 (2004).
[7]M. Furakawa and S. Tokuda, Nucl. Fusion **45**, 377 (2005).
[8]F. L. Waelbroeck, Phys. Plasmas **3**, 1047 (1996).
[9]C. L. Wahlberg and A. Bondeson, Phys. Plasmas **7**, 923 (2000).
[10]J. P. Graves, O. Sauter, and N. N. Gorelenkov, Phys. Plasmas **10**, 1034 (2003).
[11]N. Oyama, Y. Sakamoto, A. Isayama *et al.*, Nucl. Fusion **45**, 871 (2005).
[12]Y. Sakamoto, H. Shirai, T. Fujita, S. Ide, T. Takizuka, N. Oyama, and Y. Kamada, Plasma Phys. Controlled Fusion **46**, A299 (2004).
[13]K. H. Burrell, M. E. Austin, D. P. Brennan *et al.*, Plasma Phys. Controlled Fusion **44**, A253 (2002).
[14]E. Strumberger, S. Günter, P. Merkel, S. Riondato, E. Schwarz, C. Tichmann, and H. P. Zehrfeld, Nucl. Fusion **45**, 1156 (2005).
[15]C. Angioni, A. Pochelon, N. N. Gorelenkov *et al.*, Plasma Phys. Controlled Fusion **44**, 205 (2002).
[16]M. F. F. Nave, H. R. Koslowski, S. Coda, J. Graves, M. Brix, R. Buttery, C. Challis, C. Giroud, M. Stamp, and P. de Vries, Phys. Plasmas **13**, 014503 (2006).
[17]H. R. Koslowki, Fusion Sci. Technol. **47**, 260 (2005).
[18]I. T. Chapman, R. J. Akers, T. C. Hender, S. Saarelma, and S. E. Sharapov, *32nd EPS Conference on Plasma Phys. Tarragona, 27 June–1 July 2005* (Plasma Phys. Control. Fusion, Bristol, 2005), ECA Vol. 29C, P-2.062.
[19]J. E. Menard, M. G. Bell, R. E. Bell *et al.*, Nucl. Fusion **43**, 330 (2003).
[20]W. Kerner, J. P. Goedbloed, G. T. A. Huysmans, S. Poedts, and E. Schwarz, J. Comput. Phys. **142**, 271 (1998).
[21]A. B. Mikhailovskii and S. E. Sharapov, Plasma Phys. Controlled Fusion **42**, 57 (2000).
[22]G. T. A. Huysmans, J. P. Goedbloed, and W. Kerner, *Proceedings of the CP90 Conference on Computer Physics* (World Scientific, Singapore, 1991), p. 371.
[23]C. Gormezano, Plasma Phys. Controlled Fusion **41**, B367 (1999).
[24]A. J. Webster, H. R. Wilson, and A. M. M. Scaife, Phys. Plasmas **11**, 2135 (2004).
[25]A. B. Mikhailovskii, Plasma Phys. Controlled Fusion **40**, 1907 (1998).